Chapter 26
Control of Plate Vibrations with Artificial Neural Networks and Piezoelectricity

Onur Avci, Osama Abdeljaber, Serkan Kiranyaz, and Daniel Inman

Abstract This paper presents a method for active vibration control of smart thin cantilever plates. For model formulation needed for controller design and simulations, finite difference technique is used on the cantilever plate response calculations. Piezoelectric patches are used on the plate, for which a neural network based control algorithm is formed and a neurocontroller is produced to calculate the required voltage to be applied on the actuator patch. The neurocontroller is trained and run with a Kalman Filter for controlling the structural response. The neurocontroller performance is assessed by comparing the controlled and uncontrolled structural responses when the plate is subjected to various excitations. It is shown that the acceleration response of the cantilever plate is suppressed considerably validating the efficacy of the neurocontroller and the success of the proposed methodology.

Keywords Vibrations control · Artificial neural networks · Piezoelectricity · Plate vibrations · Smart plate

26.1 Introduction

With advancements in materials science and technology, engineering structures are getting more flexible and lighter [1–8]. Even though this can be considered as an advantage from economic stand point, the vibrations response becomes more critical for these structures [9–18]. Various engineering disciplines have been interested in controlling vibrations of engineering structures with active, semi-active, and passive methods [19–21]. Active control mechanisms use an array of sensor/actuator pairs to measure the vibration response of the structure and generate control forces for energy dissipation and response reduction.

For the vibration control of plates, the implementation of piezoelectric materials has been found efficient [22, 23] while Artificial Neural Networks have been started to be implemented with piezoelectricity. This study presented in this paper uses an updated version of the neural network based algorithm started by Ghaboussi and Joghataie [24] and upgraded by Bani-Hani [25]. In turn, a novel procedure is introduced for vibration control of flexible plates. The work presented in this paper involves the use of emulator neural networks (ENNs); design of a neurocontroller to calculate the required voltage for sensor/actuator units. In an attempt to formulate the model needed for running the simulations and designing the controller, finite difference technique is utilized on the cantilever plate response equations involving sensor/actuator piezoelectric patches for various excitations. The authors run numerical simulations for validating the model and verifying the efficacy of the active vibration control methodology.

26.2 Utilizing Finite Difference Method

For setting the boundary conditions in finite difference method, the nodes are generated outside the cantilever structure; also the nodes are divided into six set of nodes (Fig. 26.1).

O. Avci (✉) · O. Abdeljaber
Department of Civil Engineering, Qatar University, Doha, Qatar
e-mail: oavci@vt.edu

S. Kiranyaz
Department of Electrical Engineering, Qatar University, Doha, Qatar

D. Inman
Department of Aerospace Engineering, University of Michigan, Ann Arbor, MI, USA

C. Walber et al. (eds.), *Sensors and Instrumentation, Aircraft/Aerospace, Energy Harvesting & Dynamic Environments Testing, Volume 7*, Conference Proceedings of the Society for Experimental Mechanics Series,
https://doi.org/10.1007/978-3-030-12676-6_26

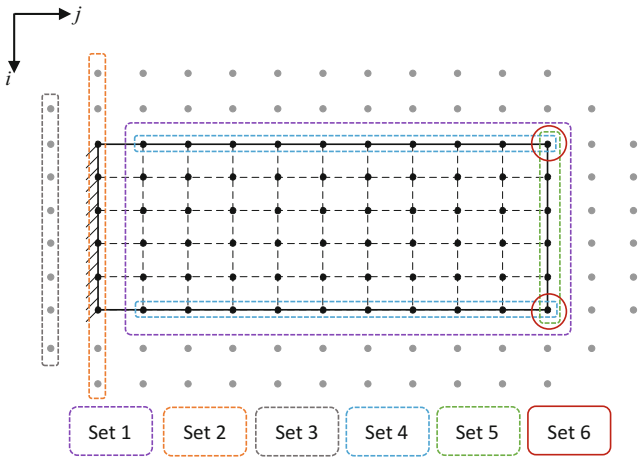

Fig. 26.1 Nodes and Node sets

26.2.1 Set 1 Nodes

Per the results of the study by Ugural [26], the equation of a rectangular thin plate subjected to time-varying dynamic excitation $P(x, y, t)$ is:

$$D\left[\frac{\partial^4 w\,(x,\,y,\,t)}{\partial x^4}+2\frac{\partial^4 w\,(x,\,y,\,t)}{\partial x^2\partial y^2}+\frac{\partial^4 w\,(x,\,y,\,t)}{\partial y^4}\right]+C_s\frac{\partial w\,(x,\,y,\,t)}{\partial t}+\rho h\frac{\partial^2 w\,(x,\,y,\,t)}{\partial t^2}=P\,(x,\,y,\,t) \tag{26.1}$$

where D is the flexural rigidity of the plate, $w(x, y, t)$ is for the deflection map of the structure at time t, C_s is the structural damping constant, ρ is the material density, and h is the thickness.

Equation (26.1) can be interpreted with the internal moments considering the fact that when N piezoelectric transducers are attached to the plate, there are external moments generated affecting the internal moments at various locations of the structure. Because the sensor/actuator units are predominantly lighter than the cantilever structure, they will have negligible effects on the dynamics of the plate. Introducing $m_x(x, y, t)$, $m_y(x, y, t)$, and $m_{xy}(x, y, t)$ for bending and twisting moments created by N piezoelectric patch units [27], the equation becomes:

$$\rho h\frac{\partial^2 w\,(x,\,y,\,t)}{\partial t^2}+C_s\frac{\partial w\,(x,\,y,\,t)}{\partial t}+D\nabla^4 w\,(x,\,y,\,t)=P\,(x,\,y,\,t)-\frac{\partial^2 m_x\,(x,\,y,\,t)}{\partial x^2}-2\frac{\partial^2 m_{xy}\,(x,\,y,\,t)}{\partial x\partial y}-\frac{\partial^2 m_y\,(x,\,y,\,t)}{\partial y^2} \tag{26.2}$$

With that, each joint is matched by one equation per Eq. (26.2) and each joints' finite difference approximation, as shown below:

$$\begin{aligned}\nabla^4 w_{(i,j,t)} \cong &\left[\frac{6}{H^4}+\frac{6}{L^4}+\frac{8}{H^2L^2}\right]w_{(i,j,t)}+\left[\frac{-4}{H^4}-\frac{-4}{H^2L^2}\right]\begin{bmatrix} w_{(i,j-1,t)}+w_{(i,j+1,t)} \\ +w_{(i-1,j,t)}+w_{(i+1,j,t)}\end{bmatrix} \\ &+\frac{2}{H^2L^2}\begin{bmatrix} w_{(i-1,j-1,t)}+w_{(i-1,j+1,t)} \\ +w_{(i+1,j-1,t)}+w_{(i+1,j+1,t)}\end{bmatrix}+\frac{1}{H^4}\begin{bmatrix} w_{(i,j+2,t)}+w_{(i,j-2,t)} \\ +w_{(i-2,j,t)}+w_{(i+2,j,t)}\end{bmatrix}\end{aligned} \tag{26.3}$$

$$\frac{\partial^2 m_{x\,(i,j,t)}}{\partial x^2}\cong\frac{-C_0 d_{31}}{h_{PZT}H^2}V(t)\left[R_{(i,j-1)}-2R_{(i,j)}+R_{(i,j+1)}\right] \tag{26.4}$$

$$\frac{\partial^2 m_y\,(i,\,j,\,t)}{\partial y^2} \cong \frac{-C_0 d_{32}}{h_{PZT} L^2} V(t)\left[R_{(i-1,\,j)} - 2R_{(i,\,j)} + R_{(i+1,\,j)}\right] \tag{26.5}$$

$$\frac{\partial^2 m_{xy}}{\partial x \partial y} = 0 \tag{26.6}$$

Inserting the Eqs. (26.3–26.6) into Eq. (26.2) results in:

$$\rho h \ddot{w}_{(i,j,t)} + C_s \dot{w}_{(i,j,t)} + D \left\{ \begin{array}{c} \left[\frac{6}{H^4} + \frac{6}{L^4} + \frac{8}{H^2 L^2}\right] w_{(i,j,t)} + \\ \left[\frac{-4}{H^4} - \frac{-4}{H^2 L^2}\right] \left[\begin{array}{c} w_{(i,j-1,t)} + w_{(i,j+1,t)} \\ + w_{(i-1,j,t)} + w_{(i+1,j,t)} \end{array}\right] + \\ \frac{2}{H^2 L^2} \left[\begin{array}{c} w_{(i-1,j-1,t)} + w_{(i-1,j+1,t)} \\ + w_{(i+1,j-1,t)} + w_{(i+1,j+1,t)} \end{array}\right] + \frac{1}{H^4} \left[\begin{array}{c} w_{(i,j+2,t)} + w_{(i,j-2,t)} \\ + w_{(i-2,j,t)} + w_{(i+2,j,t)} \end{array}\right] \end{array} \right\} = F(t) P_{(i,j)} - V(t) Z_{(i,j)} \tag{26.7}$$

$$Z_{(i,j)} = \frac{-C_0 d_{31}}{h_{PZT} H^2}\left[R_{(i,j-1)} - 2R_{(i,j)} + R_{(i,j+1)}\right] - \frac{C_0 d_{32}}{h_{PZT} L^2}\left[R_{(i-1,j)} - 2R_{(i,j)} + R_{(i+1,j)}\right] \tag{26.8}$$

26.2.2 Set 2–6 Nodes

Per [27], the equations are formed as the following:

$$\text{For Set 2}: w_{(i,j,t)} = 0 \tag{26.9}$$

$$\text{For Set 3}: w_{(i,j,t)} = w_{(i,j+2,t)} \tag{26.10}$$

$$\text{For Set 4}: (-2 - 2\upsilon)\, w_{(i,j,t)} + \upsilon\left[w_{(i,j-1,t)} + w_{(i,j+1,t)}\right] + w_{(i-1,j,t)} + w_{(i+1,j,t)} = 0 \tag{26.11}$$

$$(2\upsilon - 6)\left[w_{(i-1,j,t)} - w_{(i+1,j,t)}\right] + (2 - \upsilon)\left[w_{(i-1,j-1,t)} + w_{(i-1,j+1,t)} - w_{(i+1,j-1,t)} - w_{(i+1,j+1,t)}\right] + w_{(i-2,j,t)} - w_{(i+2,j,t)} = 0 \tag{26.12}$$

$$\text{For Set 5}: (-2 - 2\upsilon)\, w_{(i,j,t)} + \upsilon\left[w_{(i-1,j,t)} + w_{(i+1,j,t)}\right] + w_{(i,j-1,t)} + w_{(i,j+1,t)} = 0 \tag{26.13}$$

$$(2\upsilon - 6)\left[w_{(i,j+1,t)} - w_{(i,j-1,t)}\right] + (2 - \upsilon)\left[w_{(i-1,j+1,t)} + w_{(i+1,j+1,t)} - w_{(i-1,j-1,t)} - w_{(i+1,j-1,t)}\right] + w_{(i,j+2,t)} - w_{(i,j-2,t)} = 0 \tag{26.14}$$

$$\text{For Set 6}: w_{(i-1,j+1,t)} - w_{(i-1,j-1,t)} + w_{(i+1,j-1,t)} - w_{(i+1,j+1,t)} = 0 \tag{26.15}$$

26.3 State-Space Formulations

For Set 1, joints are assigned an index from 1 to n, where n is the total number of joints. With this, $R(x, y)$ can be calculated at a joint based on Eq. (26.16).

$$R\,(x,\,y) = \sum_{i=1}^{N}\left[H\left(x - x_1^i\right) - H\left(x - x_2^i\right)\right]\left[H\left(y - y_1^i\right) - H\left(y - y_2^i\right)\right] \tag{26.16}$$

For Sets 2-to-6 are the joints are matched by indices from $n + 1$ to n_t, where n_t is the sum of all joints. Forming a $2n$-dimensional state vector $\mathbf{x}\,(\mathrm{t}) = [w_1, \ldots, w_n, \dot{w}_1, \ldots, \dot{w}_n]^{\mathrm{T}}$, the system per [27] becomes:

$$\dot{\mathbf{x}}\,(\mathrm{t}) = \begin{bmatrix} \mathbf{0}_{\mathrm{n}} & \mathbf{I}_{\mathrm{n}} \\ -\mathbf{M}^{-1}\mathbf{K} & -\mathbf{M}^{-1}\mathbf{C} \end{bmatrix} \mathbf{x}\,(\mathrm{t}) + \begin{bmatrix} \mathbf{0}_{\mathrm{n}} \\ \mathbf{M}^{-1} \end{bmatrix} \left\{ F(t) \begin{bmatrix} P_1 \\ P_2 \\ \vdots \\ P_n \end{bmatrix} - V(t) \begin{bmatrix} Z_1 \\ Z_2 \\ \vdots \\ Z_n \end{bmatrix} \right\} \tag{26.17}$$

$$\mathbf{y}\,(\mathrm{t}) = \begin{bmatrix} \mathbf{0}_{\mathrm{n}} & \mathbf{I}_{\mathrm{n}} \end{bmatrix} \mathbf{x}\,(\mathrm{t}) + [\mathbf{0}_n] \left\{ F(t) \begin{bmatrix} P_1 \\ P_2 \\ \vdots \\ P_n \end{bmatrix} - V(t) \begin{bmatrix} Z_1 \\ Z_2 \\ \vdots \\ Z_n \end{bmatrix} \right\} \tag{26.18}$$

where $\boldsymbol{y}(t)$ is the state-space output.

26.4 Piezoelectric Sensor Formulation

Based on previous work [28, 29], the voltage produced by a piezoelectric sensor is:

$$V_s(t) = R_p r \int_{y_1}^{y_2} \int_{x_1}^{x_2} \left(e_{31} \frac{\partial^2 \dot{w}}{\partial x^2} + e_{32} \frac{\partial^2 \dot{w}}{\partial y^2} + 2e_{36} \frac{\partial^2 \dot{w}}{\partial x \partial y} \right) dx dy \tag{26.19}$$

The state-space system for the unit output becomes:

$$\begin{aligned} \dot{\mathbf{x}}\,(\mathrm{t}) &= \begin{bmatrix} \mathbf{0}_{\mathrm{n}} & \mathbf{I}_{\mathrm{n}} \\ -\mathbf{M}^{-1}\mathbf{K} & -\mathbf{M}^{-1}\mathbf{C} \end{bmatrix} \mathbf{x}\,(\mathrm{t}) + \begin{bmatrix} \mathbf{0}_{\mathrm{n}} \\ \mathbf{M}^{-1} \end{bmatrix} \{F(t)\mathbf{P} - V(t)\mathbf{Z}\} \\ \mathbf{y}_{\mathbf{v}}\,(\mathrm{t}) &= R_p r \mathbf{N}_{(1\times n)} \mathbf{S}_{(n\times n)} \begin{bmatrix} \mathbf{0}_{\mathrm{n}} & \mathbf{I}_{\mathrm{n}} \end{bmatrix} \mathbf{x}\,(\mathrm{t}) + 0 \times \{F(t)\mathbf{P} - V(t)\mathbf{Z}\} \end{aligned} \tag{26.20}$$

In Eq. (26.20), $\mathbf{y}_{\mathbf{v}}(\mathrm{t})$ is the updated state-space output that is equal to $V_s(t)$. The final model will house a large number high-frequency dynamics; therefore, a model reduction is needed.

26.5 Model Reduction and Kalman Filter Design

The reduced model can be defined as the following:

$$\begin{aligned} \dot{\mathbf{x}}_{\mathbf{r}}\,(\mathrm{t}) &= \mathbf{A}_r \mathbf{x}_{\mathbf{r}}\,(\mathrm{t}) + \mathbf{B}_{\mathbf{r}}\,\{F(t)\mathbf{P} - V(t)\mathbf{Z}\} \\ \mathbf{y}_{\mathbf{v}_{\mathbf{r}}}\,(\mathrm{t}) &= \mathbf{C}_r \mathbf{x}_{\mathbf{r}}\,(\mathrm{t}) + \mathbf{D}_r \times \{F(t)\mathbf{P} - V(t)\mathbf{Z}\} \end{aligned} \tag{26.21}$$

The neurocontroller created for this work (Fig. 26.2) is based on the control of the lowest (first) natural frequency of the plate. For generating the data needed to train the ENNs, a regulated output vector $\boldsymbol{z}(t)$ is formed to calculate the response for the first state:

$$z(t) = \mathbf{C}_z \mathbf{x}_{\mathbf{r}}\,(\mathrm{t}) + \mathbf{D}_z \times \{F(t)\mathbf{P} - V(t)\mathbf{Z}\} \tag{26.22}$$

The Kalman filter is defined as the following, per [27]:

$$\dot{\widehat{\mathbf{x}}}_{\mathbf{r}}\,(\mathrm{t}) = \mathbf{A}_r \widehat{\mathbf{x}}_{\mathbf{r}}\,(\mathrm{t}) + \mathbf{B}_{\mathbf{r}}\mathbf{u}\,(\mathrm{t}) + \mathbf{L}\left[y_{v_r}(t) - \mathbf{C}_r \widehat{\mathbf{x}}_{\mathbf{r}}\,(\mathrm{t}) - \mathbf{D}_r \mathbf{u}\,(\mathrm{t}) \right] \tag{26.23}$$

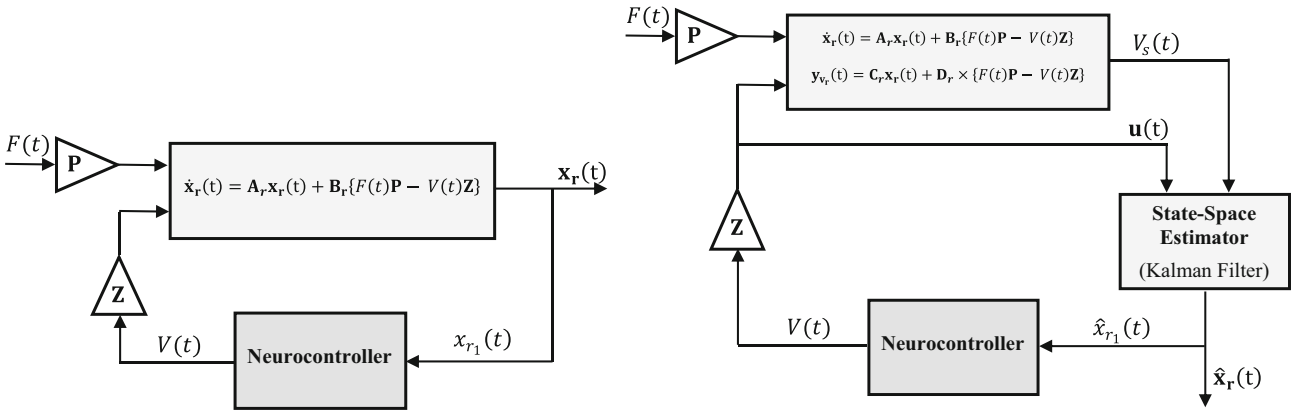

Fig. 26.2 Preliminary implementation of the Neurocontroller (left) and implementation of the Kalman Filter (right)

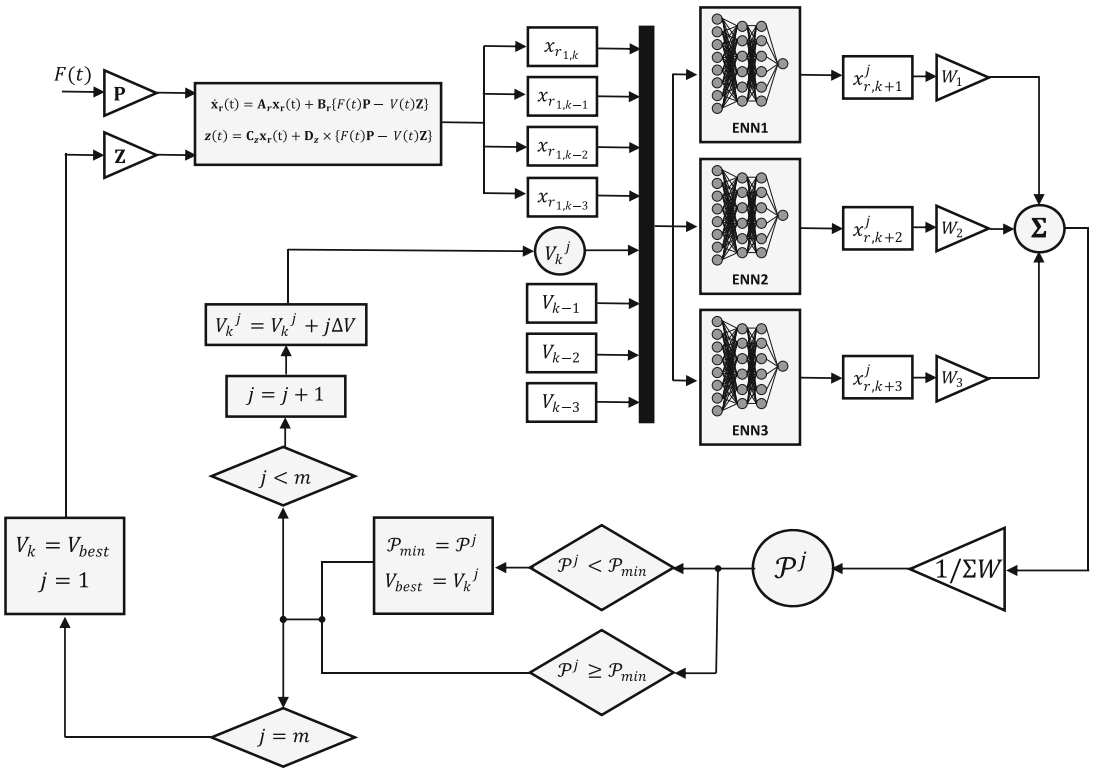

Fig. 26.3 The neurocontrol algorithm

As shown in Fig. 26.2, the initial scheme of the control algorithm is upgraded with the Kalman Filter.

26.6 The Neurocontroller

The neurocontroller training is performed on the multi-layer feedforward ENNs which are generated to compute the structural response. The neurocontrol algorithm is presented in Fig. 26.3. It is expected from the neurocontroller to generate the control voltage based on the immediate past values of the controlled state. In other words, the neurocontroller is trained to learn the transfer function from the controlled state for which the training data is produced by applying an excitation to the plate by white-noise signal and calculate the needed voltage based on the neurocontrol algorithm. With that, the data is classified in terms of input-output format, and an ANN learning algorithm is used for the training of the neurocontroller [27].

26.7 Numerical Example of a Plate with Sensor/Actuator Pair

For the numerical simulation of the thin cantilever structure with patches, the following information is used: plate dimensions $a = 0.5$ m, $b = 0.5$ m, and $h = 1.78$ mm; for material properties, the density is $\rho = 7800\text{kg/m}^3$, modulus of elasticity is $E = 200$ GPa, and Poisson's ratio is $\nu = 0.3$. The flexural rigidity is $D = 103.3$. Modal damping ratio for all modes is used as $\zeta = 0.006$. The dimensions of the patch are 6.67cm $\times$ 6.67cm with a thickness $h_{PZT} = 1$ mm. For the sensor/actuator pair, the material properties are $p_{pe} = 7650$ kg/m^3, $E_{PZ} = 63$ GPa, and $\nu_{PZT} = 0.30$. The strain constants are $d_{31} = d_{32} = 166 \times 10^{-12}$m/V, and the stress constants are $e_{31} = e_{32} = 10.46$m/V. The sensor and actuator patches are located at the same place, however, on the two opposite sides of the thin plate.

The authors wrote a MATLAB code to use finite difference technique to produce the Kalman Filter and the state-space system. The code uses Eq. (26.20) applying the MATLAB tools [30] eliminating the states with considerably small observability. As a next step, the Kalman Filter gain $\mathbf{L}$ is calculated. For the numerical simulation, the plate mesh size is $H \times L = 0.0167\text{m} \times 0.0167\text{m}$. The full state space model response and the reduced-order model response subjected to a white noise excitation are presented in Fig. 26.4. For verification purposes, the reduced-order state-space system frequencies are compared to the frequencies published by Plunkett [31] and the FE model predictions by Abaqus 6.12 [32]. All three methods frequencies are in perfect match as shown in [27].

26.7.1 Emulator Neural Network Training

A Simulink model is built to produce the training data for which the sampling period is $\Delta t = 0.001$ s and three excitations are used.

1. A uniformly distributed load is used to excite the structure for 10 seconds within a range of 0–60 Hz white noise signal.
2. A 0–5 Hz white noise signal is used to excite the piezoelectric patch for 10 seconds.
3. A uniformly distributed random load is used to excite the structure for 10 seconds while the actuator is subjected to a random voltage for 10 seconds.

Based on the above, the actual response is compared to the ENN predicted response in Fig. 26.5.

26.7.2 Evaluation of the Neurocontroller

The structural response controlled by the neurocontroller is simulated with three excitation cases:

1. A localized pulse force is applied at the point $x = 0.4$ m, $y = 0.25$ m (Fig. 26.6).
2. A distributed load is used to excite the within a range of 0–40 Hz white noise (Fig. 26.7).

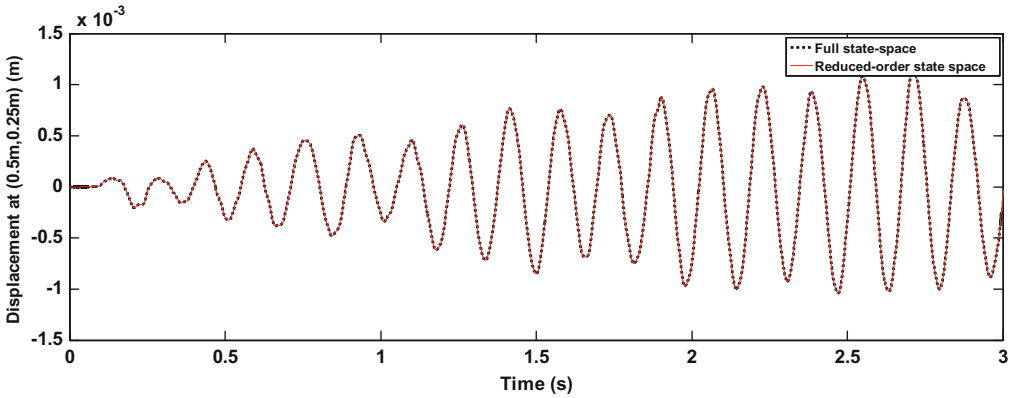

Fig. 26.4 The full state space response and the reduced-order state space response subjected to white noise

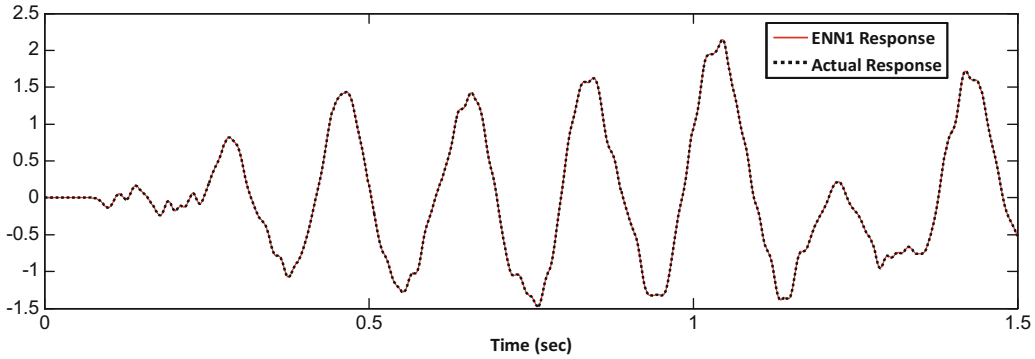

Fig. 26.5 The actual response and the emulator neural network predicted response

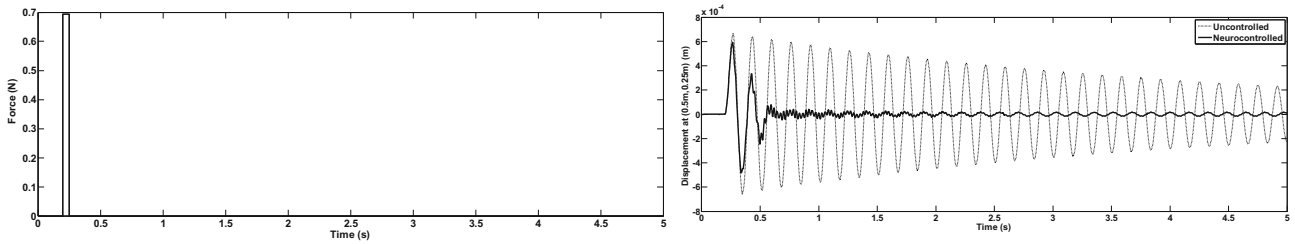

Fig. 26.6 Time histories: Load Case 1 signal (left); Uncontrolled and Neurocontrolled displacement response (right)

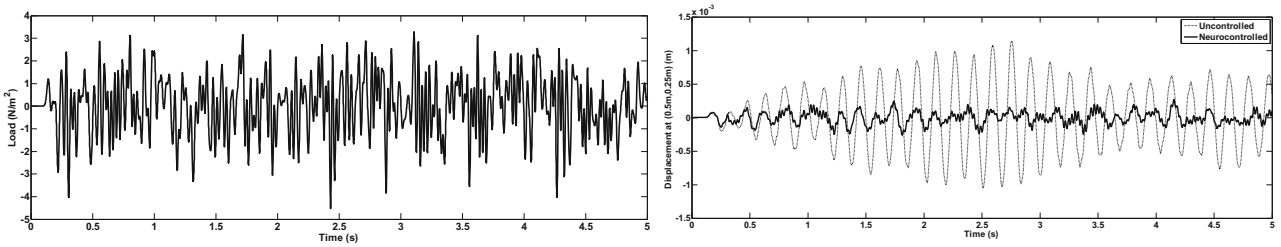

Fig. 26.7 Time histories: Load Case 2 signal (left); Uncontrolled and Neurocontrolled displacement response (right)

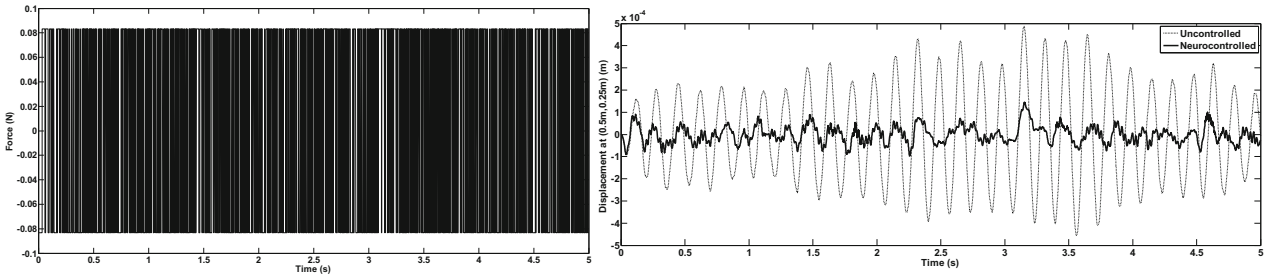

Fig. 26.8 Time histories: Load Case 3 signal (left); Uncontrolled and Neurocontrolled displacement response (right)

3. Two localized forces with varying magnitudes per pseudo random binary sequence is applied at the points $x = 0.4$ m, $y = 0.1$ m and $x = 0.4$ m, $y = 0.4$ m (Fig. 26.8).

For these excitations, the structural response is calculated at the point $x = 0.5$ m, $y = 0.25$ m (i.e. the center of the cantilever tip). Uncontrolled and neurocontrolled displacement responses are presented in Figs. 26.6, 26.7 and 26.8.

26.8 Conclusions

In this paper, the response of a thin cantilever plate structure with piezoelectric patches is studied. The first excitation was used to assess the performance of the neurocontroller in suppressing pulse loads. It is verified for this load that the response of the plate structure is reduced considerably; indicating that the proposed active control procedure is successful. The forced excitations of the second and the third load cases reveal that the proposed active control procedure is successful again. It can be concluded that the trained neurocontroller is efficient in active control of thin cantilever plates, for various kind of excitations.

References

1. Younis, A., Avci, O., Hussein, M., Davis, B., Reynolds, P.: Dynamic forces induced by a single pedestrian: a literature review. Appl. Mech. Rev. **69**, (2017). https://doi.org/10.1115/1.4036327
2. Celik, O., Do, N.T., Abdeljaber, O., Gul, M., Avci, O., Catbas, F.N.: Recent issues on stadium monitoring and serviceability: a review. In: Conference Proceedings of the Society for Experimental Mechanics Series (2016). https://doi.org/10.1007/978-3-319-29763-7_41
3. Barrett, A.R., Avci, O., Setareh, M., Murray, T.M.: Observations from vibration testing of in-situ structures. In: Proceedings of the Structures Congress Expo (2006). https://doi.org/10.1061/40889(201)65
4. Chaabane, M., Ben Hamida, A., Mansouri, M., Nounou, H.N., Avci, O.: Damage detection using enhanced multivariate statistical process control technique. In: 2016 17th International Conference on Sciences and Techniques of Automatic control & Computer Engineering STA 2016 – Proceedings (2017). https://doi.org/10.1109/STA.2016.7952052
5. Mansouri, M., Avci, O., Nounou, H., Nounou, M.: Iterated square root unscented Kalman Filter for nonlinear states and parameters estimation: three DOF damped system. J. Civ. Struct. Heal. Monit. **5**, (2015). https://doi.org/10.1007/s13349-015-0134-7
6. Mansouri, M., Avci, O., Nounou, H., Nounou, M.: A comparative assessment of nonlinear state estimation methods for structural health monitoring. In: Conference Proceedings of the Society for Experimental Mechanics Series (2015). https://doi.org/10.1007/978-3-319-15224-0_5
7. Mansouri, M., Avci, O., Nounou, H., Nounou, M.: Iterated square root unscented Kalman Filter for state estimation – CSTR model. In: 12th International Multi-Conference on Systems, Signals and Devices, SSD 2015 (2015). https://doi.org/10.1109/SSD.2015.7348243
8. Mansouri, M., Avci, O., Nounou, H., Nounou, M.: Parameter identification for nonlinear biological phenomena modeled by S-systems. In: 12th International Multi-Conference on Systems, Signals and Devices, SSD 2015 (2015). https://doi.org/10.1109/SSD.2015.7348187
9. Avci, O., Bhargava, A., Al-Smadi, Y., Isenberg, J.: Vibrations serviceability of a medical facility floor for sensitive equipment replacement: evaluation with sparse in-situ data. Pract. Period. Struct. Des. Constr. **24**, (2018)
10. Do, N.T., Gul, M., Abdeljaber, O., Avci, O.: Novel framework for vibration serviceability assessment of stadium grandstands considering durations of vibrations. J. Struct. Eng. (United States). **144**, (2018). https://doi.org/10.1061/(ASCE)ST.1943-541X.0001941
11. Avci, O., Abdeljaber, O., Kiranyaz, S., Hussein, M., Inman, D.J.: Wireless and real-time structural damage detection: a novel decentralized method for wireless sensor networks. J. Sound Vib. **424**, 158–172 (2018)
12. Avci, O., Abdeljaber, O., Kiranyaz, S., Inman, D.: Vibration suppression in metastructures using zigzag inserts optimized by genetic algorithms. In: Conference Proceedings of the Society for Experimental Mechanics Series (2017). https://doi.org/10.1007/978-3-319-54735-0_29
13. Abdeljaber, O., Avci, O., Kiranyaz, M.S., Boashash, B., Sodano, H., Inman, D.J.: 1-D CNNs for structural damage detection: verification on a structural health monitoring benchmark data. Neurocomputing. **275**, 1308–1317 (2018). https://doi.org/10.1016/j.neucom.2017.09.069
14. Abdeljaber, O., Younis, A., Avci, O., Catbas, N., Gul, M., Celik, O., Zhang, H.: Dynamic testing of a laboratory stadium structure. Geotech. Struct. Eng. Congr. **2016**, 1719–1728 (n.d.). https://doi.org/10.1061/9780784479742.147
15. Abdeljaber, O., Avci, O.: Nonparametric structural damage detection algorithm for ambient vibration response: utilizing artificial neural networks and self-organizing maps. J. Archit. Eng. (2016). https://doi.org/10.1061/(ASCE)AE.1943-5568.0000205
16. Abdeljaber, O., Avci, O., Kiranyaz, S., Gabbouj, M., Inman, D.J.: Real-time vibration-based structural damage detection using one-dimensional convolutional neural networks. J. Sound Vib. **388**, 154–170 (2017). https://doi.org/10.1016/j.jsv.2016.10.043
17. Abdeljaber, O., Avci, O., Do, N.T., Gul, M., Celik, O., Necati Catbas, F.: Quantification of structural damage with self-organizing maps. In: Conference Proceedings of the Society for Experimental Mechanics Series (2016). https://doi.org/10.1007/978-3-319-29956-3_5
18. Davis, B., Avci, O.: Simplified vibration response prediction for slender monumental stairs. In: Structures Congress 2014 – Proceedings of Structures Congress 2014 (2014). https://doi.org/10.1061/9780784413357.223
19. Inman, D.J.: Vibration with control, Wiley (2006). https://doi.org/10.1002/0470010533
20. Abdeljaber, O., Avci, O., Kiranyaz, S., Inman, D.J.: Optimization of linear zigzag insert metastructures for low-frequency vibration attenuation using genetic algorithms. Mech. Syst. Signal Process. **84**, (2017). https://doi.org/10.1016/j.ymssp.2016.07.011
21. Abdeljaber, O., Avci, O., Inman, D.J.: Optimization of chiral lattice based metastructures for broadband vibration suppression using genetic algorithms. J. Sound Vib. (2015). https://doi.org/10.1016/j.jsv.2015.11.048
22. Caruso, G., Galeani, S., Menini, L.: Active vibration control of an elastic plate using multiple piezoelectric sensors and actuators. Simul. Model. Pract. Theory. **11**, 403–419 (2003). https://doi.org/10.1016/S1569-190X(03)00056-X
23. Qiu, J., Haraguchi, M.: Vibration control of a plate using a self-sensing piezoelectric actuator and an adaptive control approach. J. Intell. Mater. Syst. Struct. **17**, 661–669 (2006). https://doi.org/10.1177/1045389X06055760
24. Ghaboussi, J., Joghataie, A.: Active control of structures using neural networks. J. Eng. Mech. **121**, 555–567 (1995). https://doi.org/10.1061/(ASCE)0733-9399(1995)121:4(555)
25. Bani-Hani, K., Ghaboussi, J.: Nonlinear structural control using neural networks. J. Eng. Mech. **124**, 319–327 (1998). https://doi.org/10.1061/(ASCE)0733-9399(1998)124:3(319)

26. Ugural, A.C.: Stresses in beams, plates, and shells (2010). https://doi.org/10.1007/s13398-014-0173-7.2
27. Abdeljaber, O., Avci, O., Inman, D.J.: Active vibration control of flexible cantilever plates using piezoelectric materials and artificial neural networks. J. Sound Vib. **363**, (2016). https://doi.org/10.1016/j.jsv.2015.10.029
28. Tavakolpour, A.R., Mailah, M., Mat Darus, I.Z., Tokhi, O.: Self-learning active vibration control of a flexible plate structure with piezoelectric actuator. Simul. Model. Pract. Theory. **18**, 516–532 (2010). https://doi.org/10.1016/j.simpat.2009.12.007
29. Quek, S.T., Wang, S.Y., Ang, K.K.: Vibration control of composite plates via optimal placement of piezoelectric patches. J. Intell. Mater. Syst. Struct. **14**, 229–245 (2003). https://doi.org/10.1177/1045389X03034686
30. The Mathworks Inc., MATLAB – MathWorks, www.Mathworks.Com/Products/Matlab (2016)
31. Plunkett, R.: Natural frequencies of uniform and non-uniform rectangular cantilever plates. J. Mech. Eng. Sci. **5**, 146–156 (1963). https://doi.org/10.1243/JMES_JOUR_1963_005_020_02
32. Dassault Systèmes Simulia, Fallis, A., Techniques, D.: ABAQUS documentation, Abaqus 6.12. (2013). https://doi.org/10.1017/CBO9781107415324.004